MARTIN MARIETTA

MML TR 93-01

Tensile Study of Single-Crystal Ternary $L1_2$ Trialuminide $Al_{66}Ti_{25}Mn_9$

Contract #F49620-91-C-0099

Final Report

S. A. Brown and K. S. Kumar

Prepared for:

Air Force Office of Scientific Research
Bolling Air Force Base
Washington, D. C. 20332-6448

Submitted by:

Martin Marietta Laboratories
1450 South Rolling Road
Baltimore, MD 21227-3898

MML TR 93-01

Tensile Study of Single-Crystal Ternary $L1_2$ Trialuminide $Al_{66}Ti_{25}Mn_9$

Contract #F49620-91-C-0099

Final Report

S. A. Brown and K. S. Kumar

Prepared for:

Air Force Office of Scientific Research
Bolling Air Force Base
Washington, D. C. 20332-6448

Submitted by:

Martin Marietta Laboratories
1450 South Rolling Road
Baltimore, MD 21227-3898

COMPLETED PROJECT SUMMARY

TITLE: "Tensile Study of Single-Crystal Ternary $L1_2$ Trialuminide $Al_{66}Ti_{25}Mn_9$"

PRINCIPAL INVESTIGATOR: K. Sharvan Kumar, Manager, Composites Dept.

INCLUSIVE DATES: 1 Sept. 1991 to 31 Jan. 1993

CONTRACT/GRANT NUMBER: F49620-91-C-0099

SENIOR RESEARCH PERSONNEL: K. S. Kumar, Manager, Composites Dept.

JUNIOR RESEARCH PERSONNEL: S. A. Brown, Associate Specialist R/D

PUBLICATIONS:

"Mechanical Behavior of $L1_2$ Single Crystal $Al_{66}Ti_{25}Mn_9$," S. A. Brown, D. P. Pope and K. S. Kumar, presented at Mat. Res. Soc. Conf. Symp. L, Nov. 30 to Dec. 4, 1992, Boston, MA. To appear in High-Temperature Ordered Intermetallics V, Vol. 288, Materials Research Society, Pittsburgh, PA.

ABSTRACT OF OBJECTIVES AND ACCOMPLISHMENTS:

Single crystal $Al_{66}Ti_{25}Mn_9$ has been produced and tested in compression as well as uniaxial tension. Yield strengths in compression for orientations near [001] and $[\bar{1}11]$ continuously decrease with increasing temperature in a manner similar to other single crystal $L1_2$ trialuminides, and also to polycrystals of these materials. Slip was determined to occur on the {111} octahedral planes using two-surface analysis. Critical resolved shear stress (CRSS) variation with temperature, calculated for the $(111)[\bar{1}01]$ slip system, overlaps closely for both orientations. Dislocation analysis confirmed the Burgers vectors to be of the type a<110> at both 298K and 1073K. A few uniaxial tension tests were conducted near [001] at 1073K; the specimens which had been hot isostatically pressed contained a small amount of residual porosity and second phases which resulted in elastic failure even at this high temperature. Efforts to produce additional crystals with better microstructure for tension testing are in progress.

REPORT DOCUMENTATION PAGE

Form Approved
OMB No. 0704-0188

1. AGENCY USE ONLY (Leave blank)	2. REPORT DATE	3. REPORT TYPE AND DATES COVERED
	Mar. 2, 1993	FINAL REPORT, 9/1/91 to 1/31/93

4. TITLE AND SUBTITLE
Tensile Study of Single-Crystal Ternary $L1_2$ Trialuminide $Al_{66}Ti_{25}Mn_9$

5. FUNDING NUMBERS
61102F 2306 A1

6. AUTHOR(S)
S. A. Brown and K. S. Kumar

7. PERFORMING ORGANIZATION NAME(S) AND ADDRESS(ES)
Martin Marietta Corporation
1450 South Rolling Road
Baltimore, Maryland 21227-3898

8. PERFORMING ORGANIZATION REPORT NUMBER
MML TR 93-01

9. SPONSORING/MONITORING AGENCY NAME(S) AND ADDRESS(ES)
AFOSR/NE
Building 410, Bolling AFB DC
20332-6448

10. SPONSORING/MONITORING AGENCY REPORT NUMBER
F49620-91-C-0099

11. SUPPLEMENTARY NOTES

12a. DISTRIBUTION/AVAILABILITY STATEMENT
APPROVED FOR PUBLIC RELEASE: DISTRIBUTION IS UNLIMITED.

12b. DISTRIBUTION CODE

13. ABSTRACT (Maximum 200 words)

Single crystal $Al_{66}Ti_{25}Mn_9$ has been produced and tested in compression as well as uniaxial tension. Yield strengths in compression for orientations near [001] and [$\bar{1}$11] continuously decrease with increasing temperature in a manner similar to other single crystal $L1_2$ trialuminides, and also to polycrystals of these materials. Slip was determined to occur on the {111} octahedral planes using two-surface analysis. Critical resolved shear stress (CRSS) variation with temperature, calculated for the (111)[$\bar{1}$01] slip system, overlaps closely for both orientations. Dislocation analysis confirmed the Burgers vectors to be of the type a<110> at both 298K and 1073K. A few uniaxial tension tests were conducted near [001] at 1073K; the HIPed specimens contained a small amount of residual porosity and second phases, which resulted in elastic failure even at this high temperature. Efforts to produce additional crystals with even better microstructures for tension testing are underway.

14. SUBJECT TERMS	15. NUMBER OF PAGES
	27
	16. PRICE CODE

17. SECURITY CLASSIFICATION OF REPORT	18. SECURITY CLASSIFICATION OF THIS PAGE.	19. SECURITY CLASSIFICATION OF ABSTRACT	20. LIMITATION OF ABSTRACT
UNCLASSIFIED	UNCLASSIFIED	UNCLASSIFIED	

TABLE OF CONTENTS

ABSTRACT

Single crystal $Al_{66}Ti_{25}Mn_9$ has been produced and tested in compression as well as uniaxial tension. Yield strengths in compression for orientations near [001] and [$\bar{1}$11] continuously decrease with increasing temperature in a manner similar to other single crystal $L1_2$ trialuminides, and also to polycrystals of these materials. Slip was determined to occur on the {111} octahedral planes using two-surface analysis. Critical resolved shear stress (CRSS) variation with temperature, calculated for the (111)[$\bar{1}$01] slip system, overlaps closely for both orientations. Dislocation analysis confirmed the Burgers vectors to be of the type a<110> at both 298K and 1073K. A few uniaxial tension tests were conducted near [001] at 1073K; the specimens which had been hot isostatically pressed contained a small amount of residual porosity and second phases, which resulted in elastic failure even at this high temperature. Efforts to produce additional crystals with better microstructure for tension testing are in progress.

I. INTRODUCTION

The continually growing demand for lightweight, high temperature materials for structural applications in hypersonic transportation has led to a focus on such refractory materials as ordered intermetallics, ceramics, and composites thereof. Typical applications include the nose cone and leading edge of wing structures, engine components such as turbine blades, combustor and nozzle sections, and missile fins. Ordered intermetallics are promising candidates for such applications based on their high melting points and inherent limited diffusion. Additionally, the low densities offered by aluminum-rich ternary intermetallics coupled with their potentially good oxidation resistance make them especially attractive for these applications.

Ternary $L1_2$ trialuminides have been evaluated over the past few years for their potential as high temperature structural materials. They possess a desirable cubic structure, as opposed to their non-cubic DO_{22} and DO_{23} binary trialuminide counterparts. The $L1_2$ trialuminide alloys based on Al-Ti-X contain ~8-12 at.% of X, where X can be Cu, Ni, Fe, Mn, Cr, Pd, Ag or some combination of these elements. Mechanical properties of this family of alloys has largely been evaluated, and only the Mn- and Cr-containing trialuminides have been shown to exhibit any room temperature ductility. In-depth studies of these two compounds led to the conclusion that the Mn-containing compound, $Al_{66}Ti_{25}Mn_9$, had a better balance of strength, ductility and oxidation resistance.

In polycrystalline form, $Al_{66}Ti_{25}Mn_9$ exhibited an intermediate temperature ductility minimum at around 773K. Its ambient temperature ductility was measured to be 0.2%, while at 1073K, 5% elongation was recorded. It was argued that the low ambient temperature ductility and the ductility minimum in polycrystalline $Al_{66}Ti_{25}Mn_9$ may arise from limited slip transfer across grain boundaries at low temperatures, and environmental embrittlement of grain boundaries at intermediate temperatures,

respectively. Further, it was proposed that tensile studies of single crystal $Al_{66}Ti_{25}Mn_9$ would isolate these effects. If this theory is correct, the ductility exhibited by single crystals of $Al_{66}Ti_{25}Mn_9$ would be higher than that of polycrystals over the low and intermediate temperature ranges.

The aim of this study has been to grow single crystals of $Al_{66}Ti_{25}Mn_9$ and to test them in uniaxial tension as a function of temperature and orientation, and to characterize the operative slip systems and dislocation dissociation schemes. Difficulties were encountered initially in growing good quality crystals--porosity and small amounts of second phases persisted. As a result, a significant portion of the program was directed at obtaining good quality crystals by optimizing growth parameters, alloy composition modifications and microstructural characterization. During the initial period, compression studies were, however, performed and these results are included in the report. More recently, improved quality single crystals have been grown; tensile studies are on-going and further results will be provided as they come in. In the next chapter, a literature review of progress on the microstructural characterization and mechanical behavior of $L1_2$ trialuminides is presented. Chapter III documents the proposed tasks, and the experimental procedure adopted is included in Chapter IV. Observations and the discussion of results constitute Chapter V, and conclusions from the study are drawn in the last chapter.

II. LITERATURE REVIEW

A. Binary Trialuminides

Transition metal elements from groups IVA (Ti, Zr, Hf) and VA (V, Nb, Ta) form binary compounds of the type Al_3X, which possess either the DO_{22} structure or its related long period superlattice, DO_{23}. These crystal structures may be constructed from an $L1_2$ lattice through the introduction of 1/2<110> displacement vectors on selected (001) planes in the $L1_2$ structure (Fig. 1). These Al_3X compounds melt either congruently or by means of a peritectic reaction at temperatures ranging from 1343K - 1950K; they often exist as line compounds, making it near impossible to produce them as single-phase materials. Further, aluminum is in equilibrium with these compounds, and residual amounts present in the microstructure will melt preferentially at low temperatures. In a recent review of ternary Al-rich intermetallics (1), it was concluded that while intersolubility between two Al_3X-type compounds was possible in the pseudobinary section of the ternary space, the line compound nature was essentially retained, implying that alloying is not likely to ease processing constraints. An exception is the Al-Ti-Mo system, where the compositional range of existence of Al_3Ti is significantly enhanced by Mo addition (up to ~20 at.% Mo was dissolved in Al_3Ti while retaining the DO_{22} structure). In trying to make these trialuminides more ductile, microalloying approaches were examined. For example, the compressive strain-to-failure in Al_3Ti was increased through additions of B, Li, Zr and Hf (2), and also the extent of twinning in Al_3V was increased by the substitution of a small amount (~1 at.%) of titanium for vanadium (3). Nevertheless, only modest improvements in compressive ductility were observed.

In addition to the transition metal elements just mentioned (groups IVA and VA), two group IIIA elements, Sc and Y, and the rare earth elements, Er, Yb, Ho, Np, Pu, Tm, Lu and U, form trialuminide compounds, four of which possess the $L1_2$ ordered structure:

Al_3Sc, Al_3Er, Al_3Yb and Al_3U. From melting point and density considerations, Al_3Sc is the most attractive of these compounds, although the high cost of Sc precludes widespread use. Table I lists melting point, density and crystal structure for many of the binary trialuminides. Theoretical and experimental research on the $L1_2$ trialuminide Al_3Sc has produced much information on this compound. First principles calculations of the elastic moduli of Al_3Sc (4) were found to be in good agreement with experimental data generated using ultrasonic techniques (5), Table II. Compression behavior of cast and homogenized Al_3Sc containing ~500 ppm oxygen was characterized in the range 77K - 1273K (6). Strength at 77K was marginally higher than at room temperature, and a mild positive temperature dependence was observed above room temperature with a strength peak at ~500K. Failure was by brittle transgranular cleavage along {110}- and {100}-type planes, although the strength remained below 150 MPa at all temperatures. Fracture toughness of Al_3Sc was estimated to be ~3 MPa $\sqrt{m}$ at room temperature, and the brittle fracture was attributed to a low K/G ratio (bulk to shear modulus), consistent with the Pugh Criterion (7), and a low K value implies a low cleavage strength for these materials, consistent with the observed fracture mode.

B. Ternary $L1_2$ Trialuminides

1. Phase Equilibria

The $L1_2$, DO_{22} and DO_{23} crystal structures (Fig. 1) are related by periodically arrayed displacement vectors of the type a/2<110>, as noted earlier. Theoretically, by changing {001} antiphase boundary energies, the stability of a compound may be reversibly altered from the DO_{22} to the $L1_2$ structure, leading to a possibility of alloying the binary trialuminides to stabilize the more symmetric $L1_2$ structure. Earlier research efforts of various groups in the Soviet Union and Germany had identified ternary aluminum-rich $L1_2$ compounds in the Al-Ti-Cu, Al-Ti-Ni and Al-Ti-Fe systems with

compositions of the form Al_5Ti_2Cu, $Al_{67}Ti_{25}Ni_8$ and $Al_{22}Ti_8Fe_3$; and more recently, similar compounds have been shown to exist in the Al-Ti-Cr, Al-Ti-Mn, Al-Ti-Pd and Al-Ti-Ag systems. Also, Al-rich $L1_2$ compounds are present in the Al-Zr-X (X=Cu, Ni, Fe, Co) and Al-Hf-Cu systems. These systems may be thought of as being macroalloyed versions of the DO_{22} trialuminides, since both phases are seen to be in close proximity upon examination of the ternary isotherms. Phase equilibria in these systems was recently reviewed (1), and this section includes only those systems pertinent to the current effort (8-16). The Al-rich, ternary $L1_2$ compounds are typically found within a phase field only a few atomic percent in size, even at high temperatures, with melting points comparable to Al_3Ti or Al_3Zr (Table I) and densities <4.0 g/cm^3 (for the Ti-containing compounds). These $L1_2$ compounds are currently believed to be derived from binary Al_3X (X=Ti, Zr, Hf) by alloying, although some arguments have also been put forth that relate them to binary Al_2X (X=Ti, Zr, Hf).

Markiv et al. studied the phase equilibria of the three ternary systems Al-Ti-Cu, Al-Ti-Ni, and Al-Ti-Fe at 1073K (8). In the Al-Ti-Fe system, they identified three ternary phases, one of which was an $L1_2$ compound of the formula 25Ti-9Fe-66Al (at.%) with lattice parameter 0.3981 nm. Later, Seibold investigated the same system (9); however, she not only generated the Al-Ti-Fe isotherm at 1073K, but the liquidus projection and the entire reaction summary in the ternary system as well as the respective binary systems. She also found three ternary intermetallics in this system, one being an $L1_2$ compound of the form $Ti_8Al_{22}Fe_3$, which confirms the composition that Markiv et al. had identified. Her study, however, produced a lattice parameter of 0.393 nm and may have been a result of her marginally different composition. The melting point of this ternary $L1_2$ compound was 1603K, later confirmed by other researchers (10).

More recent work on the systems Al-Ti-Cu, Al-Ti-Ni and Al-Ti-Fe by Mazdiyasni et al. (11) attempted to pinpoint the phase boundaries for the Al-rich $L1_2$ compound in each of these systems. In comparing the $L1_2$ phase field in the Al-Ti-Fe system at 1473K vs.

1073K, they noticed that it did not shrink concentrically at the lower of the two temperatures, but was skewed towards the Al-rich corner (Fig. 2). The ramifications of this feature lie in reproducibly attaining the composition of interest, while avoiding second phase precipitation during cooling. A composition of 64Al-28Ti-8Fe (at.%) was given for the geometric center of the single phase field. Their work in the Al-Ti-Ni system produced a 1473K isotherm that gives the center of the $L1_2$ phase field as 66Al-27Ti-7Ni (at.%). The extent of the phase field is only a few atomic percent in any direction, which is in good agreement with Raman and Schubert (12) and Huang et al. (13). From this work it is apparent that the $L1_2$ phase field exists to as high as 1473K, contrary to the observations of Nash et al. (14) that this phase forms only by a solid state reaction below 1273K.

Similarly, ternary $L1_2$ compounds have been located in the Al-Ti-Mn and Al-Ti-Cr systems. Mabuchi et al. (15) reported an $L1_2$ composition of $Al_{66}Ti_{25}Mn_9$; their phase diagram, generated at 1273K, shows this cubic phase to be in equilibrium with Al_3Ti, Al_2Ti, TiAl, $TiAl_2Mn$ and MnAl (Fig. 3a). Its lattice parameter was given as 0.3955 nm. At the same time, Zhang et al. (16) independently reported on the existence of the $L1_2$ phase in both the Al-Ti-Mn and Al-Ti-Cr systems. Subsequently, they (17) determined the $L1_2$ phase field in the Mn-based system at 1473K (Fig. 3b); it was reported as being much larger than the 1273K phase field (15), which is to be expected at a higher temperature. The frequent presence of very fine precipitates of Al_2Ti at ambient temperature (18) for materials with target compositions in the single phase region defined by the 1273K isotherm, i.e. $Al_{66}Ti_{25}Mn_9$ (15), leads to the conclusion that the size of the $L1_2$ phase field is likely to decrease further at lower temperatures. According to Mabuchi et al. (15), the size of the $L1_2$ phase field at 1273K is only about 1 or 2 at.% in width; thus attaining and even measuring compositions with such accuracy is nontrivial. There appears to be no phase diagram data at low temperatures in these systems, presumably due to the difficulty in measuring the composition of the $L1_2$

compound. This is a direct consequence of the Al_2Ti phase precipitating in the matrix $L1_2$ phase with a fine interwoven "tweed" morphology.

2. Mechanical Properties and Dislocation Observations

Various mechanical properties of these Al-rich $L1_2$ alloys have been measured including hardness, strength, and ductility in compression and bending. Compression behavior of the $L1_2$ compound in the Al-Ti-Fe system has been studied by Wu et al. (19). Polycrystals and single crystals were tested as a function of temperature, composition and orientation to determine compressive strength and ductility. Compression studies on a homogenized polycrystalline alloy of composition 64.6Al-9.7Fe-25.7Ti (at.%) showed a mild positive temperature dependence of strength from room temperature to 800K, where strength levels were in the 300-350 MPa range for several strain rates (1.75×10^{-4} s^{-1} to 1.75×10^{-3} s^{-1}). From 77K to room temperature there was a sharp decrease in yield strength, beginning around 450 MPa at 77K. Above 800K, strength dropped off continuously to 1273K where strengths between 200-250 MPa were recorded. Profuse microcracking in the specimens led to substantial apparent compressive ductility, even at low temperatures; three-point bend tests, however, failed to produce any room temperature plastic strain in this material. Wu et al. (20) also produced single crystals of this material. Slip trace analysis on polished compression specimens showed that {111} octahedral slip predominated at most temperatures and orientations; specimens oriented near $[\bar{1}11]$ additionally exhibited cube slip lines. Compositions with higher Ti-contents were much stronger than those with lower amounts, and cracked more readily under loading. Greater yield stresses were thought to be only due to solid solution strengthening, but were later also attributed to the presence of the Al_2Ti phase, which is often only observable in the transmission electron microscope.

Dislocation structures and dissociations were examined in $Al_{67}Fe_8Ti_{25}$ by Inui et al. (21) after deformation at room temperature and 873K. Room-temperature

dissociation was determined to occur by splitting of the superdislocation into a/3<112> partials, coupled by a superlattice intrinsic stacking fault (SISF). At 873K, near-edge a/2<110> superpartials connected by an antiphase boundary (APB) were seen on the cube planes. Low-temperature dissociation schemes were substantiated by a contrast analysis of a/3<112> partials where the relative intensities, weak or strong, were attributed to a difference in the Burgers vectors of the partial dislocations. A typical dissociation reaction is: $a[101] = a/3[112] + a/3[2\bar{1}1]$, where it may be noted that the a/3<112> type partials will always be different to equate to an a<110> type total dislocation, thus asymmetrical contrast is anticipated to originate from the differing partials. Contrast analysis of these dissimilar partials is questioned by Veyssiere and Morris (22) who argue that these asymmetrical contrast features are entirely consistent with an APB-dissociation mechanism. Veyssiere and Morris state that asymmetrical images of partial dislocations occur very commonly when a dislocation splits into collinear partials, such as a/2<110> connected by APB, and they provided evidence of this fact. They claimed that even in the paper by Inui et al. (21) there are numerous contrast features supportive of the APB-dissociation scheme. Arguments put forth by Veyssiere and Morris are indeed convincing and lead to agreement with their conclusion that insufficient evidence was provided by Inui et al. to substantiate the claim of SISF-bounded superpartials at low temperatures.

Recent computer simulations by Zhang et al. (23) of superpartial-pair contrast produced in the electron microscope demonstrate that an APB-dissociated superdislocation as well as its SISF counterpart can lead to asymmetrical intensities of the partials. Increasing asymmetry at closer partial spacings was also supported by the simulations, as would be the case for material deformed at low temperatures where the spacing is expected to be on the order of 2-5 nm. It was emphasized that *in-situ* annealing experiments performed by Morris (24) also agree with their observations. He annealed a foil of room-temperature-deformed $Al_{64}Fe_8Ti_{28}$, leading to partial spacings

that increased with annealing time and temperature, with a concomitant loss of partial dislocation contrast asymmetry.

Dislocation observations have been made in most of the other $L1_2$ trialuminides. Vasudevan et al. (25) imaged dislocations in $Al_{67}Ni_8Ti_{25}$ using 2-nm-resolution weak-beam microscopy and reported dissociated a<110> superdislocations only at higher temperatures (573K - 873K), where a/2<110> type partials were seen on the (001) planes. Many dipoles were reported, which is likely responsible for rapid work hardening observed during deformation. Powers and Wert (26) were not able to resolve any superpartials if they were present in $Al_{67}Pd_8Ti_{25}$. Dipoles were not observed in homogenized material, but many were introduced into the microstructure after plastic deformation. George et al. (5) observed a<110> superdislocations on {111} planes in Al_3Sc and $Al_{66}Fe_6V_5Ti_{23}$ with partial dislocation identities of a/2<110> with connecting APB. Partial spacings of 3.7 nm for Al_3Sc and 4 nm in the quaternary intermetallic were measured.

Dislocation characteristics aside, mechanical properties of the $L1_2$ trialuminide systems containing Mn and Cr have proven to be the best of the Al-Ti-X family, both having been reported to display ambient temperature ductility in some type of tensile deformation mode. Zhang et al. reported four-point bend ductility in $Al_{66}Ti_{25}Cr_9$ and $Al_{66}Mn_6Ti_{23}V_5$, but not $Al_{67}Ti_{25}Mn_8$ using polished specimens (16). Uniaxial tension tests performed by Kumar and Brown on $Al_{66}Ti_{25}Mn_9$ and $Al_{67}Ti_{25}Cr_8$ confirmed that only the $Al_{66}Ti_{25}Mn_9$ showed ambient tensile ductility in 30μm grain size material tested in the as-forged condition (27, 28). Ambient temperature ductility in the Mn-containing alloy was confirmed by Chen et al. (29). The tension tests by Kumar and Brown (28) showed $Al_{67}Ti_{25}Cr_8$ to have ductility >0.2% at temperatures above ~823K, which increased to ~19% at 1073K. In contrast, $Al_{66}Ti_{25}Mn_9$ displayed 0.2% tensile ductility at ambient temperature (27). Ductility in the Mn-containing trialuminide, measured at 0.2% at ambient temperature, increased to 1.3% at 623K, then decreased to 0.3% at 773K,

and subsequently increased again to ~5% at 1073K (Fig. 4). This observed ductility minimum was attributed to a possible grain boundary embrittlement. Further, transmission electron microscopy (TEM) observations led them to suggest that dislocation transmission through grain boundaries at low temperatures could have been difficult, limiting slip behavior, and that grain boundaries, if removed, would also perhaps eliminate the intermediate temperature ductility minimum.

Thus, to verify the validity of these suggestions, this program was aimed at growing single crystals of $Al_{66}Ti_{25}Mn_9$ and evaluating this intermetallic in compression and in tension as a function of temperature and crystallographic orientation. Further, transmission electron microscopy techniques combined with two-surface slip trace analysis were intended to identify operating slip systems and dislocation dissociation schemes.

III. PROPOSED EXPERIMENTAL TASKS

1. Cast a sufficient amount of $Al_{66}Ti_{25}Mn_9$, homogenize the ingot(s) to obtain substantially single phase material, and characterize them in terms of composition and microstructure. If necessary, forge these ingot(s) into 1-in-high pancakes to ensure good-quality, fully dense starting material.

2. A. Grow a sufficient amount of single-crystal material at the University of Pennsylvania to perform the tests outlined in the remaining tasks.
   B. Characterize the microstructure and crystallography of the single-crystal material using X-ray diffraction and optical metallography techniques.

3. A. Machine a sufficient number of buttonhead tensile specimens in two predetermined orientations.
   B. Perform duplicate tensile tests at room temperature, 473K, 623K, 773K, 923K and 1073K. Measure yield strength, ductility and fracture strength.

4. A. Cut thin foil specimens from deformed samples for dislocation analysis, and determine dislocation dissociation and types of faults present.
   B. Compare results obtained in this study with previous results on polycrystalline material and with similar studies performed in compression on single-crystal $Al_{66}Ti_{25}Mn_9$ in another ongoing Air Force Program at the University of Pennsylvania.

5. Document methods and results in a semi-annual progress report and a final report to AFOSR at the end of the program.

IV. EXPERIMENTAL PROCEDURE

A. Single Crystal Growth

One large 3-kg ingot of $Al_{66}Ti_{25}Mn_9$ was induction melted using high-purity binary master alloys and cast into a graphite mold. Cylinders (19 mm dia.) that were suitable to use as starting materials for single crystal growth were electrodischarge-machined (EDM) from the ingot. The procedure for growing single crystals involves loading a tapered alumina crucible with a conical tip into the Bridgeman furnace, and slowly heating in vacuum to 1273K, allowing proper outgassing of the crucible and metal. Subsequently the chamber is backfilled with argon before melting. From this stage, a modified Bridgeman method was used, which involved slowly lowering the crucible tip into the temperature gradient zone of the furnace, followed by slow cooling of the entire furnace. Initially a number of trials were made to obtain optimal growth parameters for producing a substantial length of single-crystal material. The time-temperature schedule in Table III was most successful in producing the single crystals. Several such crystals that were grown in the early part of this program contained a low volume fraction of second phase. In an attempt to achieve target composition, small pieces of Al-65 wt.% Ti master alloy and/or pure Al were also added in small amounts to the crucible. Once the appropriate growth parameters and alloy composition were established, about a 50% success rate was maintained for obtaining a good-sized single crystal. A photograph of one such specimen is shown in Fig. 5.

B. Single Crystal Evaluation

Crystals were sectioned by EDM and analyzed with Laue backscattered X-ray diffraction for crystallographic orientation. Optical microscopy on etched crystals was used to verify the absence of secondary grains. Top and bottom surfaces of large crystal

segments were checked by the Laue technique in several locations to verify its single crystal nature. Optical microscopy and limited energy-dispersive X-ray (EDX) analysis were used to characterize minor second phases present in the microstructure, although extensive phase characterization was beyond the scope of this program. Wet chemical analysis was performed on some crystals in more than one location to determine compositional uniformity.

C. Compression and Tension Specimen Preparation

Compression specimens (3 mm square x 6.5 mm) were machined by EDM from a single crystal whose growth axis was 27° from [001], near the middle of the stereographic triangle. Compressive axes for the specimens were selected to be ~10° off [001] and ~10° off [$\bar{1}$11] (Fig. 6). Several individual compression specimens were oriented using Laue backscattered X-ray diffraction to confirm that they shared a common compressive axis. Sides of the specimens were mechanically polished to allow observation of slip bands after testing. Specimens were tested from 77K to 1073K using an Instron testing machine at a constant crosshead speed of ~8.5 x 10^{-4} mm/s, corresponding to an approximate initial strain rate of 1.3 x 10^{-4} s^{-1}. Tests were terminated at about 2% strain, and thus, compressive strain-to-failure was not measured. Two-surface slip trace analysis was used to determine the operative slip planes. Yield stresses were measured at 0.2% strain and critical resolves shear stresses (CRSS) were calculated for the operative slip planes. Dislocation analysis was performed on ~[001] compression specimens deformed at 298K and 1073K. Burgers vectors were identified using $\mathbf{g} \cdot \mathbf{b}$ contrast analysis.

Crystals from which tensile specimens were obtained had undergone a HIP cycle of 4 hours at 1473K and 104 MPa. One-inch long tensile specimens were machined from these crystals in a flat tensile specimen geometry (Fig. 7). A "soft" test orientation

was chosen (Fig. 6) to maximize the likelihood of recording tensile ductility. The specimens were mechanically polished to a 3μm finish, and the corners were slightly rounded to avoid premature failure from stress concentrations. Tensile specimens were tested at 1073K on an Instron testing machine with specially made Inconel grips at a constant crosshead speed of ~8.4 x 10^{-4} mm/s, corresponding to a strain rate of ~1 x 10^{-4} s^{-1}. The gage surface was examined optically for slip traces, while the fracture surface was studied using scanning electron microscopy (SEM).

V. RESULTS AND DISCUSSION

A. Crystal microstructure

Initial crystals that were grown were found to have small amounts of various second phases. Among them was the Al_2Ti phase, which can appear in dimensions ranging from 50μm in length to submicron size (Fig. 8a). Near small pores in the as-grown crystals are limited amounts of rod-shaped precipitates likely to be Al_3Ti (Fig. 8b) based on work by Wu (30). Another phase, which is believed to be stabilized by nitrogen--Ti_2AlN, was also found, most often segregated by gravity to the bottom conical section of the crystals (Fig. 8c). While these phases typically predominate on the Al-Ti rich side of the $L1_2$ phase field, an interdendritic Mn-rich phase is observed on the Al-Mn rich side, which may be continuous if the volume fraction is large enough (Fig. 8d). Away from these localized second phases (except for Al_2Ti, which is more homogeneously distributed when present) is a predominantly single-phase microstructure (Fig. 8e).

The interdendritic phase in Fig. 8d could not be dissolved by homogenization and was determined by energy dispersive X-ray (EDX) analysis to be 57Al-40Mn-3Ti (at.%). Examination of the Al-Ti-Mn isotherm at either 1273K or 1473K (Fig. 3a,b) revealed that this Mn-rich phase is likely in equilibrium with the $L1_2$ phase (nominally $Al_{66}Ti_{25}Mn_9$). Additions of Al and Ti were made (1 to 5 wt.% total) to subsequently-grown crystals in an effort to eliminate this interdendritic phase. One such modified crystal containing 1.6 g. Al and 3 g. Ti additions was found to be free of the interdendritic phase, but examination of a thin foil of this material in the transmission electron microscope (TEM) revealed a microstructure with a large fraction of Al_2Ti platelets. Clearly, the $L1_2$ phase field is very restricted at lower temperatures and it has proven to be extremely difficult to remove all deleterious second phases in these crystals. No matter what compensation was made,

the presence of one or both phases was the result. Our task then became to minimize the amount of second phase present to produce a material best capable of achieving tensile ductility. The large interdendritic phase was expected to limit ductility the most due to its interconnected morphology; thus, elimination of this phase became the revised goal, at the likely expense of introducing a small amount of the Al_2Ti phase. Crystals with an acceptable balance of second phases were eventually attained.

Representative chemical analysis of the single crystals is given in Table IV. An examination of Table IV reveals excess Ti at the bottom portion of the crystal, where a much higher volume fraction of second phase was found (Fig. 8c). These features suggest gravity segregation of Ti-rich precipitates (e.g. Ti_2AlN) that are likely present in the molten metal and settle during solidification. This portion of the crystal is never used. The middle and top portions of the crystals gave similar chemical analyses and were thus uniform in composition.

Examination of single crystal surfaces in several locations showed their orientations to be identical within experimental error, as expected. Over the length of a crystal, ~25 mm, its orientation tended to rotate by a degree or two as observed in many other single crystals, due to the presence of low-angle boundaries. Given the small size of specimens, this effect did not influence mechanical properties or slip trace observations in any measurable amount.

B. Compression Testing

Compression tests in this study were performed on specimens obtained from a crystal containing some amounts of the interdendritic phase, described above. This phase, in small amounts was not expected to significantly influence compressive yield strength measurements, whereas, in tension, this brittle phase (forming a semi-continuous network) would undoubtedly lead to premature failure. In contrast, small

amounts of fine Al_2Ti platelets will significantly influence the compressive yield stress, but, in restricted quantities may not significantly influence tensile ductility, particularly at higher temperatures, where they may dissolve, their solubility being dictated by the slope of the $L1_2$ / $L1_2$ + Al_2Ti solvus. While this is beneficial for ductility, it has important ramifications on dislocation dissociation schemes and the APB/SISF energies.

Compressive properties of single crystal $Al_{66}Ti_{25}Mn_9$ as a function of temperature were examined in two orientations using deformation axes near [001] and [$\bar{1}$11]. Yield stresses measured at 0.2% offset continuously decreased with increasing temperature, as shown in Fig. 9. This yield strength-temperature profile is similar to the behavior exhibited by other $L1_2$ trialuminides in both single crystal and polycrystal forms; however, the sharp increase in yield stress at temperatures approaching 77K as observed in the Al-Ti-Fe $L1_2$ intermetallic (19) is not as pronounced in this alloy. Two-surface slip trace analysis at various temperatures showed the slip planes to be of the {111} type for both orientations.

Representative slip traces are shown at various temperatures for the specimens tested in the **C1** orientation (Fig. 10). More than one octahedral plane was active for slip in each case, i.e. a single slip condition was not completely achieved. Schmid factors were calculated for various possible slip systems in both orientations (**C1** and **C2**), and are tabulated in Table V. Critical resolved shear stresses (CRSS) for (111)[$\bar{1}$01] slip, the primary active slip plane, were calculated, and the variation in CRSS with test temperature is given in Fig. 11. These results agree with the data for the Cr-based $L1_2$ compound (30), but are lower than those from the Fe-based intermetallic (20), whose CRSS shows a mild positive temperature dependence between room temperature and 900K, and is roughly twice that of $Al_{66}Ti_{25}Mn_9$. The Fe-based material is believed to have contained the Al_2Ti phase, which increases strength significantly. $Al_{67}Ti_{25}Cr_8$ and $Al_{66}Ti_{25}Mn_9$ were shown to have similar compressive strengths in polycrystalline form (31), and therefore it is not surprising that their CRSS profiles are similar. Dislocation

analyses performed on ~[001] specimens deformed at room temperature and 1073K using **g** • **b** contrast criteria showed Burgers vectors to be of the <110> type, as shown in Table VI. A group of dislocations is shown under various two-beam imaging conditions in Fig. 12 (298K, **C1** compression specimen), where the <110> type Burgers vector may be verified. At high temperature, the same result was obtained (Fig. 13). This Burgers vector is consistent with what is expected for an ordered fcc lattice, and agrees with all other published data on the $L1_2$ trialuminide alloys.

C. Tensile Testing

Preliminary tensile tests were conducted at 1073K on the assumption that microstructural flaws that were present (e.g. isolated "islands" of interdendritic phase, unhealed pores) would be more readily tolerated at this temperature, thereby permitting measurable ductility. The tensile axis of these specimens (**T**, Fig. 6) was only five degrees from the **C1** compression axis, which is reflected by their similar Schmid factors: **T** = 0.464, **C1** = 0.485 for $(111)[\bar{1}01]$ slip system. The best tensile test produced a fracture stress of 91 MPa, corresponding to a resolved shear stress (RSS) of 42 MPa with no measurable plasticity. The load-displacement curve for this test is shown in Fig. 14a. This resolved shear stress of 42 MPa is almost equal to the CRSS measured in compression at 1073K, which was ~45 MPa, suggesting that the tensile specimen was on the verge of yielding; however, slip lines were not observed on the polished faces of the specimen up to 1000X magnification.

A specimen tested at 1073K is shown in Fig. 14a, where it may be seen that failure occurred within the gage section. Fracture surfaces of the tensile specimens were examined using an SEM; cleavage failure was noted (Fig. 14b,c). A very smooth cleavage surface near the initiation site was typical (Fig. 14b), followed by river patterns at a greater distance from the initiation site, shown more prominently in Fig. 14c.

Improved specimen quality is clearly mandatory, even for successful high temperature testing, reflecting the extreme flaw sensitivity of these materials. Crystals recently grown, however, appear to be somewhat better than those used for preliminary testing, and will be evaluated further.

VI. SUMMARY

- Single crystals of $Al_{66}Ti_{25}Mn_9$ were successfully grown, typically ~20 mm in diameter and ~30 mm high.

- A small amount of second phase was inevitable in these crystals, irrespective of the various starting compositions evaluated. These were either Al-Mn-rich interdendritic phases or Al_2Ti solid state precipitation with a "tweed" morphology.

- Yield stress in compression was measured as a function of temperature and crystallographic orientation. The single crystal exhibits a normal temperature dependence of strength.

- Two-surface slip trace analysis showed {111} slip at all temperatures evaluated.

- Critical resolved shear stress (CRSS) was obtained as a function of test temperature.

- Burgers vectors at room temperature and 1073K were determined by **g** • **b** contrast analysis, and dislocations are of a<110> type as expected.

- Only a limited number of tensile tests have been performed to date; this is a direct consequence of the difficulty in producing satisfactory quality, single phase, single crystals necessary for tensile tests.

- Preliminary tensile tests at 1073K showed a tensile yield strength comparable to the compressive yield strength without macroscopic plasticity, confirming the need for flaw-free material.

VII. ACKNOWLEDGEMENTS

One author (S. B.) would like to thank his M.S. thesis advisor, Dr. D. P. Pope, at the University of Pennsylvania for technical advice and guidance through the project. We also gratefully acknowledge W. Romanow, R. Hsiao and the National Science Foundation (NSF) Materials Research Laboratory (MRL) program through the Laboratory for Research of the Structure of Matter (LRSM) at the University of Pennsylvania for the crystal growtn facilities. Also, we acknowledge Drs. D. Dimiduk and D. B. Miracle from the Wright Materials Laboratory of the Wright Patterson Air Force Base for assistance with hot isostatic pressing.

VIII. REFERENCES

1. K. S. Kumar, Int. Mat. Reviews **35**, pp. 293-327 (1990).
2. M. Yamaguchi, Y. Shirai and Y. Umakoshi: in "Dispersion strengthened aluminum alloys," (ed. Y.-W. Kim and W. M. Griffith), pp. 721-740; 1988, The Minerals, Metals and Materials Society, Warrendale, PA.
3. Y. Umakoshi, M. Yamaguchi, T. Yamane and T. Hirano, Philos. Mag. A **58**, pp. 651-666 (1988).
4. C. L. Fu, J. Mater. Res. **5**, pp. 971-979 (1990).
5. E. P. George, J. A. Horton, W. D. Porter and J. H. Schneibel, J. Mater. Res. **5**, pp. 1639-1648 (1990).
6. J. H. Schneibel and E. P. George, Scr. metall. mater. **24**, pp. 1069-1074 (1990).
7. S. F. Pugh, Philos. Mag. **45**, 823 (1954).
8. V. Ya. Markiv, V. V. Burnashova, and V. P. Ryabov: *Akad. Nauk Ukr. SSR, Metallofiz.* **46**, pp. 103-110 (1973).
9. A. Seibold, *Z. Metallkd.* **72**, pp. 712-719 (1981).
10. K. S. Kumar and J. R. Pickens, in "Dispersion strengthened aluminum alloys," (ed. Y.-W. Kim and W. M. Griffith), pp. 763-786; 1988, The Minerals, Metals and Materials Society, Warrendale, PA.
11. S. Mazdiyasni, D. B. Miracle, D. M. Dimiduk, M. G. Mendiratta, and P. R. Subramanian, Scr. Metall. **23**, pp. 327-331 (1989).
12. A. Raman and K. Schubert, *Z. Metallkd.* **56**, pp. 99-104 (1965).
13. S. C. Huang, E. L. Hall, and M. F. X. Gigliotti, J. Mater. Res. **3**, pp. 1-7 (1988).
14. P. G. Nash, V. Vejins, and W. W. Liang, Bull. Alloy Phase Diagrams **3**, pp. 367-374 (1982).
15. H. Mabuchi, K. Hirukawa and Y. Nakayama, Scr. metall. mater. **23**, pp. 1761-1766 (1989).
16. S. Zhang, J. P. Nic and D. E. Mikkola, Scr. metall. mater. **24**, pp. 57-62 (1990).
17. S. Zhang and D. E. Mikkola, Scr. metall. mater. **26**, pp. 1315-1320 (1992).
18. S. A. Brown, D. P. Pope and K. S. Kumar, presented at Mat. Res. Soc. Conf., Symp. L, Nov. 30 - Dec. 4, 1992, Boston, MA; to appear in High Temperature Ordered Intermetallic Alloys V, Vol. 288, Mat. Res. Soc., Pittsburgh PA.
19. Z. L. Wu, D. P. Pope and V. Vitek, Scr. metall. mater. **24**, pp. 2187-2190 (1990).
20. Z. L. Wu, D. P. Pope and V. Vitek, Scr. metall. mater. **24**, pp. 2191-2196 (1990).
21. H. Inui, D. E. Luzzi, W. D. Porter, D. P. Pope, V. Vitek and M. Yamaguchi, Philos. Mag. A **65**, pp. 245-259 (1992).

22. P. Veyssiere and D. G. Morris, accepted Philos. Mag. A (1992).
23. S. Zhang, D. E. Mikkola and W W. Milligan, Scr. metall. mater. **27**, pp. 1073-1077 (1992).
24. D. G. Morris, Philos. Mag. A **65**, pp. 389-401 (1992).
25. V. K. Vasudevan, R. Wheeler and H. Fraser, in High-Temperature Ordered Intermetallic Alloys III, Vol. 133, pp. 705-710, 1989. Mat. Res. Soc., Pittsburgh PA.
26. W. O. Powers and J. A. Wert, Metall. Trans. A **21**, pp. 145-151 (1990).
27. K. S. Kumar and S. A. Brown, Philos. Mag. A **65**, pp. 91-109 (1992).
28. K. S. Kumar and S. A. Brown, Acta metall. mater. **40**, pp. 1623-1632 (1992).
29. X. Chen, X. Wu, S. Chen and G. Hu, Scr. metall. mater. **26**, pp. 1775-1778 (1992).
30. Z. L. Wu, Ph.D. Thesis, University of Pennsylvania (1993).
31. S. A. Brown, K. S. Kumar and J. D. Whittenberger, Scr. metall. mater **24**, pp. 2001-2006 (1990).
32. C. D. Turner, W. O. Powers and J. R. Wert, Acta metall. **37**, pp. 2635-2643 (1989).
33. D. E. Mikkola, J. P. Nic, S. Zhang and W. W. Milligan, ISIJ Inter. **31**, pp. 1076-1079 (1991).

TABLE I. Physical and Crystallographic Data for some Binary Trialuminides

Compound	Density (g/cm^3)	Crystal Structure	T_m (K)	Melting Transformation
Al_3Sc	3.02	$L1_2$	1593	Peritectic
Al_3Ti	3.31	DO_{22}	1625	Peritectic
Al_3V	3.34	DO_{22}	1633	Peritectic
Al_3Zr	4.11	DO_{23}	1853	Congruent
Al_3Nb	4.52	DO_{22}	1950	Congruent
Al_3Er	5.5*	$L1_2$	1343	Peritectic
Al_3U	6.4	$L1_2$	1623	Peritectic
Al_3Ta	6.9*	DO_{22}	1825	Peritectic
Al_3Hf	----	DO_{23}**	1860	Congruent

* calculated values.

** Al_3Hf transforms to a DO_{22} structure above 935K.

TABLE II. Elastic Properties of some $L1_2$ Trialuminides

Compound	E	K	G	υ	K/G	Ref.
Al_3Sc	166	99	68	0.22	1.46	(5)
Al_3Sc*	166	90	69	0.20	1.30	(4)
$Al_{67}Ti_{25}Ni_8$	200	116	82	0.22	1.41	(32)
	188	105	78	0.20	1.3	(33)
$Al_{67}Ti_{25}Fe_8$	192	89	84	0.14	1.06	(5)
	181	90	78	0.16	1.2	(33)
$Al_{67}Ti_{25}Cr_8$	168	99	68	0.22	1.46	(5)
$Al_{67}Ti_{25}Mn_8$	174	74	79	0.11	0.9	(33)
$Al_{67}Zr_{25}Fe_8$	166	103	68	0.22	1.51	(5)

* calculated values.

TABLE III. Time-Temperature Schedule for Growing Single Crystals of $Al_{66}Ti_{25}Mn_9$

Segment	1	2	3	4	5	6	7
Temp. (K)	298	623	623	1023	1023	1273	1273
Time[1] (h)	--	4	4	4	2	4	1[2]
Segment	8	9	10	11	12	13	14
Temp. (K)	1723	1723	1683	1643	1603	1583	298[4]
Time (h)	4	3[3]	18	18	18	18	8

1 ramp time in hours to attain set temperature.
2 furnace chamber is backfilled with argon.
3 crucible is lowered into temperature gradient zone of the furnace.
4 This method does not incorporate an in-situ homogenizing step; crystals are homogenized in a separate step for 3 days at 1373K.

TABLE IV. Chemical Analyses of a Representative Single Crystal (wt.%)

Position	Al	Ti	Mn
Near Top	51.1	34.2	14.7
Middle	51.2	33.7	15.1
Bottom	45.2	44.6	10.2
'Typical'*	49-52	33-35	14.5-16

* 'Typical' denotes compositions measured in castings found free of TEM-scale Al_2Ti precipitates.

Table V. Schmid Factors for Compression Specimens

Orientation	Slip System	Schmid Factor
Near [001]	$(111)[\bar{1}01]$	0.485
	$(\bar{1}11)[101]$	0.467
	$(\bar{1}11)[0\bar{1}1]$	0.390
	$(111)[0\bar{1}1]$	0.379
Near $[\bar{1}11]$	$(111)[\bar{1}01]$	0.382
	$(111)[\bar{1}10]$	0.334
	$(\bar{1}\bar{1}1)[011]$	0.270

TABLE VI. Burgers Vectors for Dislocations Observed in $Al_{66}Ti_{25}Mn_9$ Crystals

Temp. (K)	Dislocation	Burgers Vector
298K	J	a[0$\bar{1}$1]
	K	a[0$\bar{1}$1]
	L	a[$\bar{1}$01]
	M	a[101]
	N	a[101]
	P	a[101]
1073K	A	a[101]
	B	a[0$\bar{1}$1]
	C	a[0$\bar{1}$1]
	D	a[0$\bar{1}$1]
	E	a[101]
	F	a[0$\bar{1}$1]

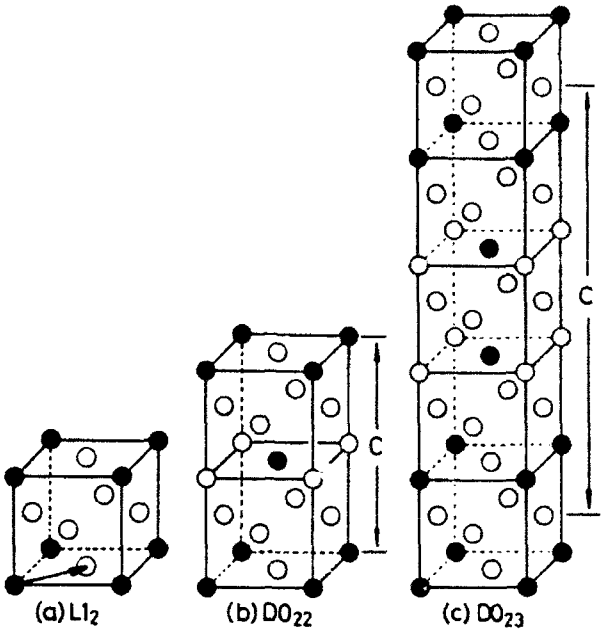

Fig. 1. Structures of the types (a) $L1_2$, (b) DO_{22}, and (c) DO_{23}, -- Yamaguchi et al. (2).

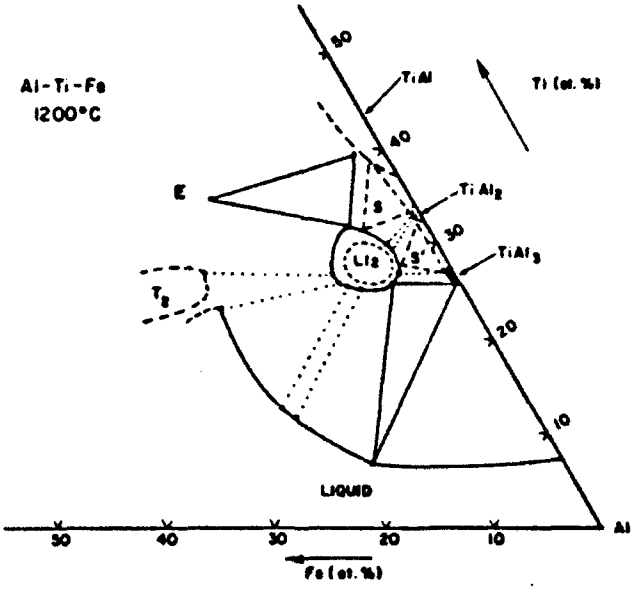

Fig. 2. Al-rich corner of the 1473K Al-Ti-Fe ternary isotherm. Dotted lines indicate two-phase tie lines; dashed circle within 1473K $L1_2$ phase field is the estimated field at 1073K, -- Mazdiyasni et al. (11).

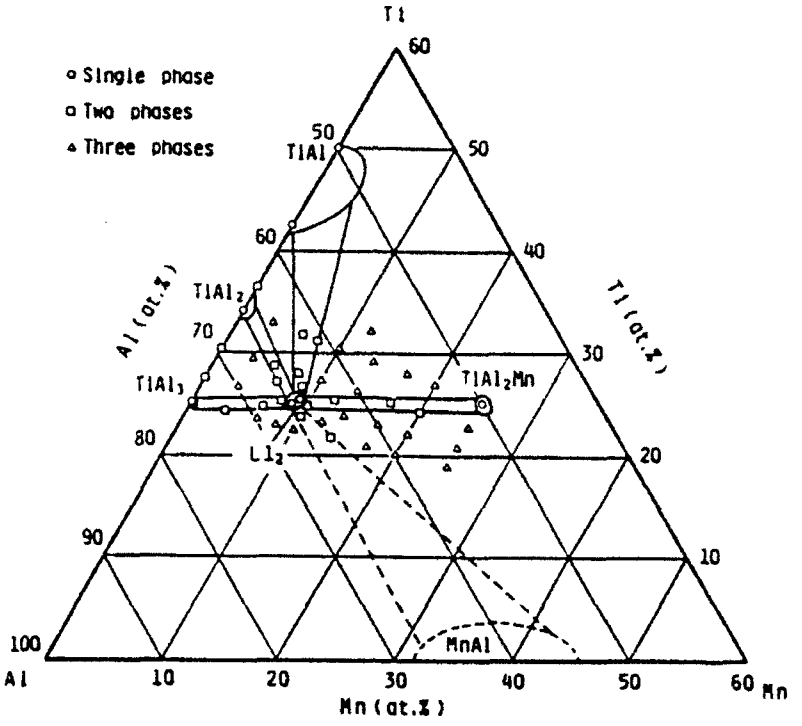

(a)

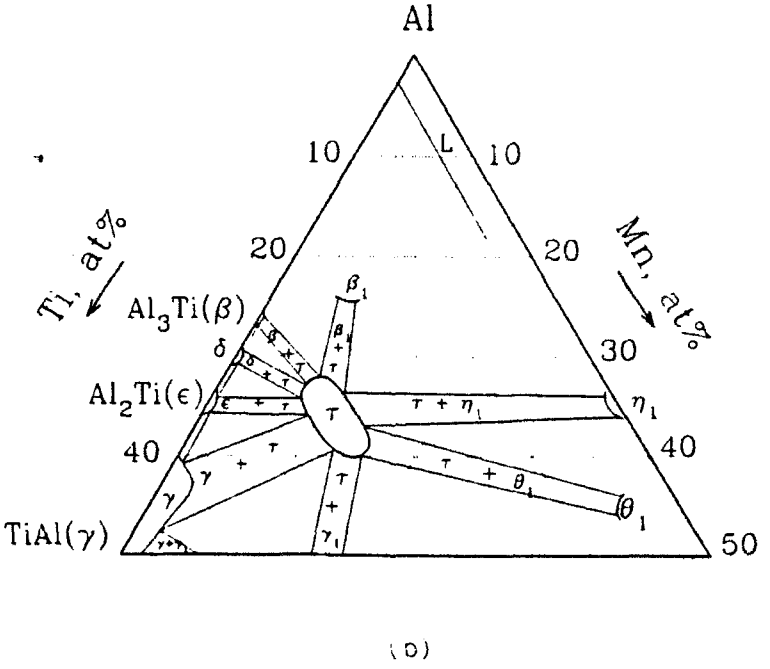

(b)

Fig. 3. Al-Ti-Mn ternary isotherm generated at (a) 1273K, from Mabuchi et al. (15), and (b) 1473K, from Zhang et al. (17).

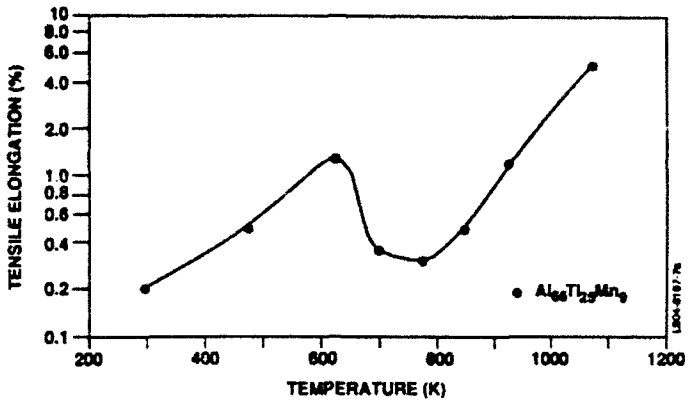

Fig. 4. Ductility vs. temperature for polycrystalline $Al_{66}Ti_{25}Mn_9$, -- Kumar and Brown (27).

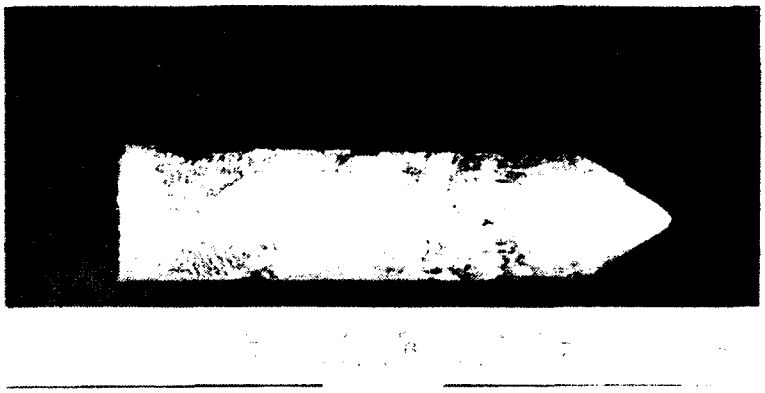

Fig. 5. Photograph of single crystal $Al_{66}Ti_{25}Mn_9$ produced for this study.

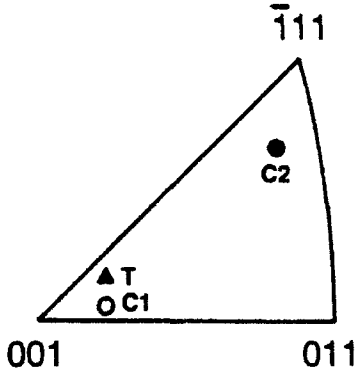

Fig. 6. Standard triangle identifying orientations of the tensile axis (**T**) and two compressive axes (**C1** and **C2**) used in this study.

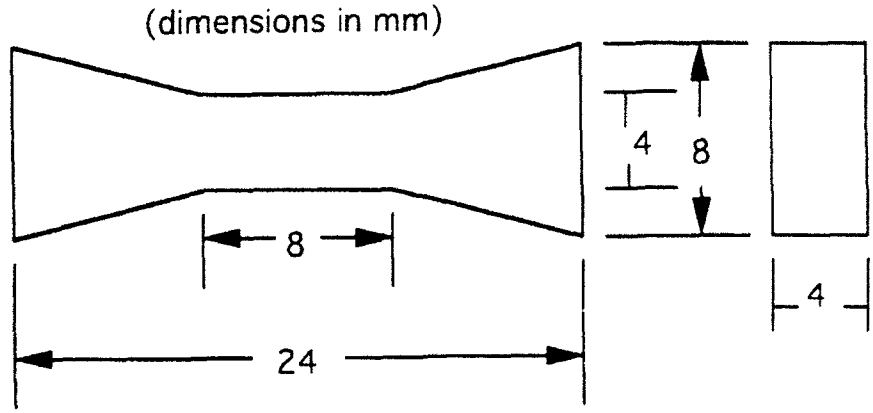

(a)

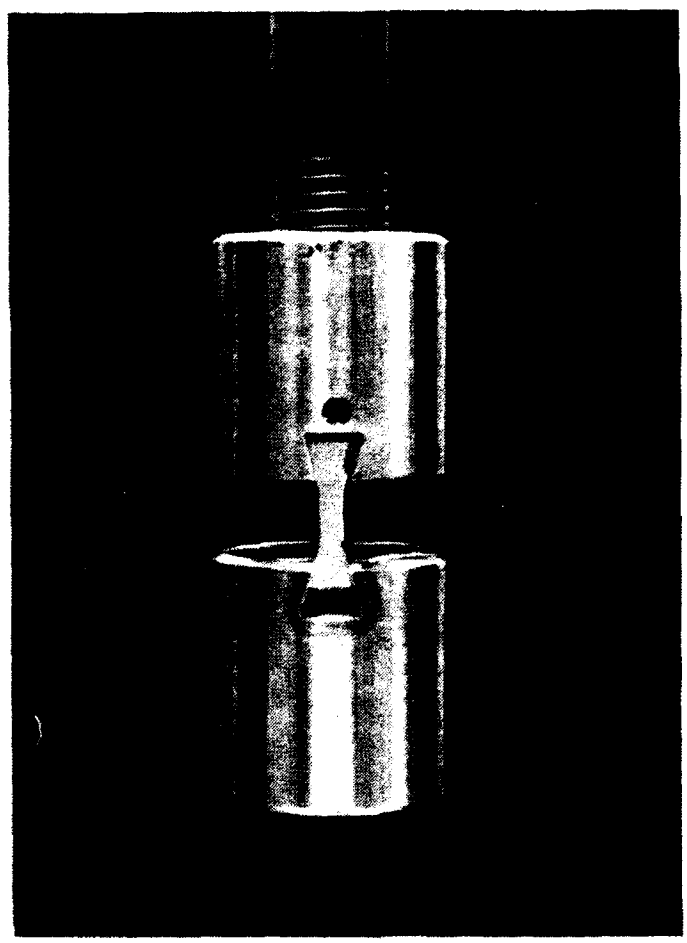

(b)

Fig. 7. (a) Schematic of flat tensile specimen geometry, and (b) tensile testing setup including specially-made Inconel grips.

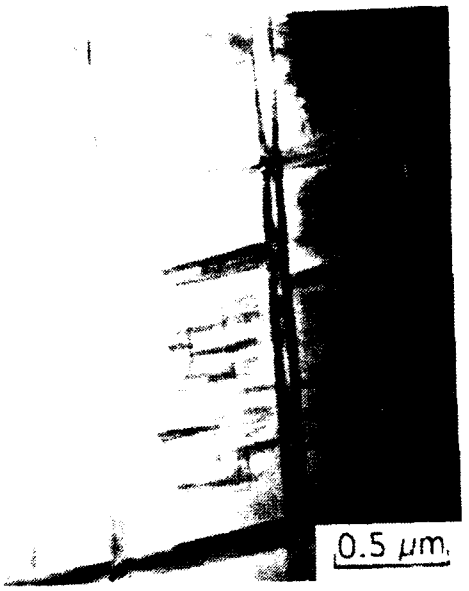

(a)

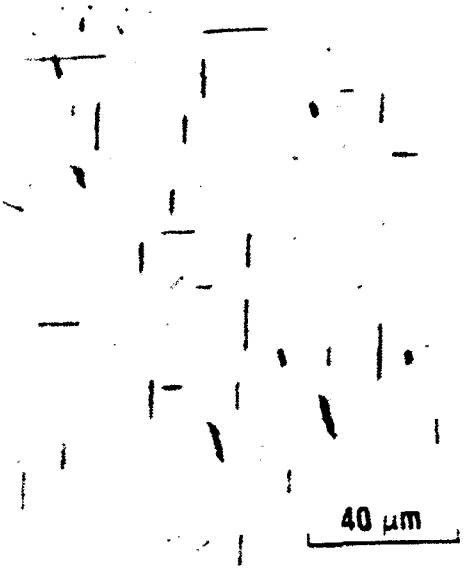

(b)

(c)

(d)

(e)

Fig. 8. Micrographs showing various second phases found in homogenized single crystals: (a) fine Al_2Ti platelets, (b) rod-shaped Al_3Ti precipitates, (c) blocky Ti_2AlN found only at tip of crystals, (d) Mn-rich interdendritic phase, and (e) clean $L1_2$ phase.

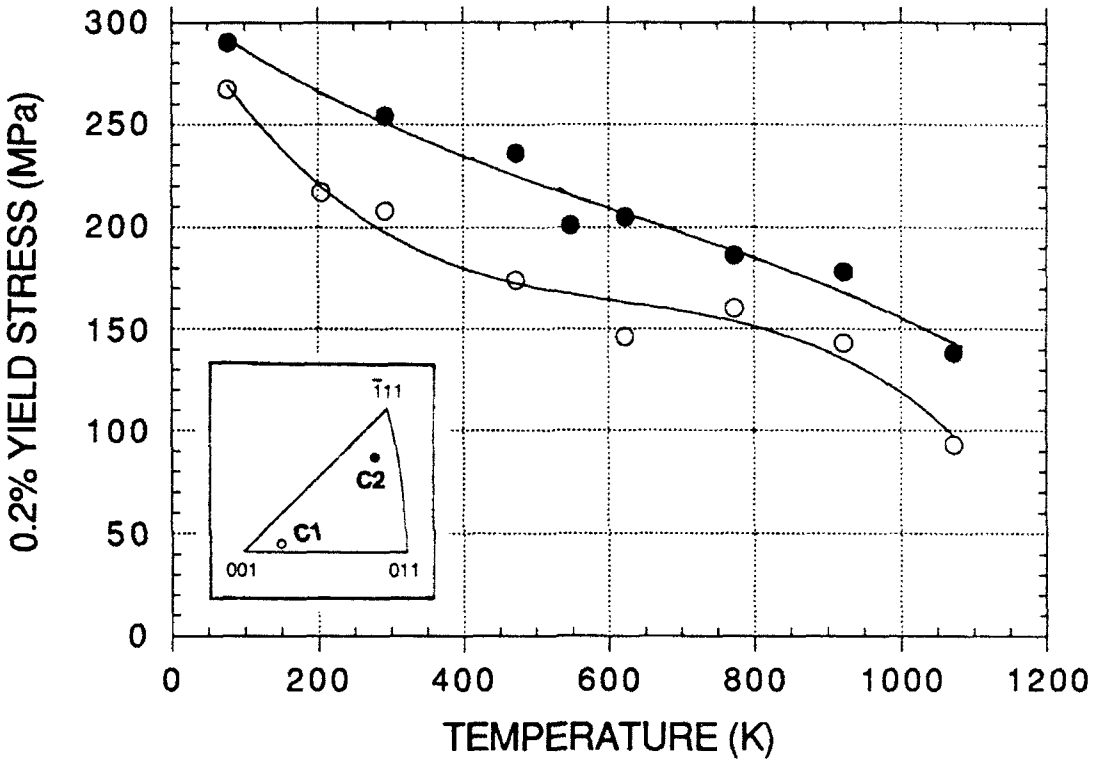

Fig. 9. Compressive yield stresses (0.2% offset) of single crystal $Al_{66}Ti_{25}Mn_9$ in two orientations as a function of temperature.

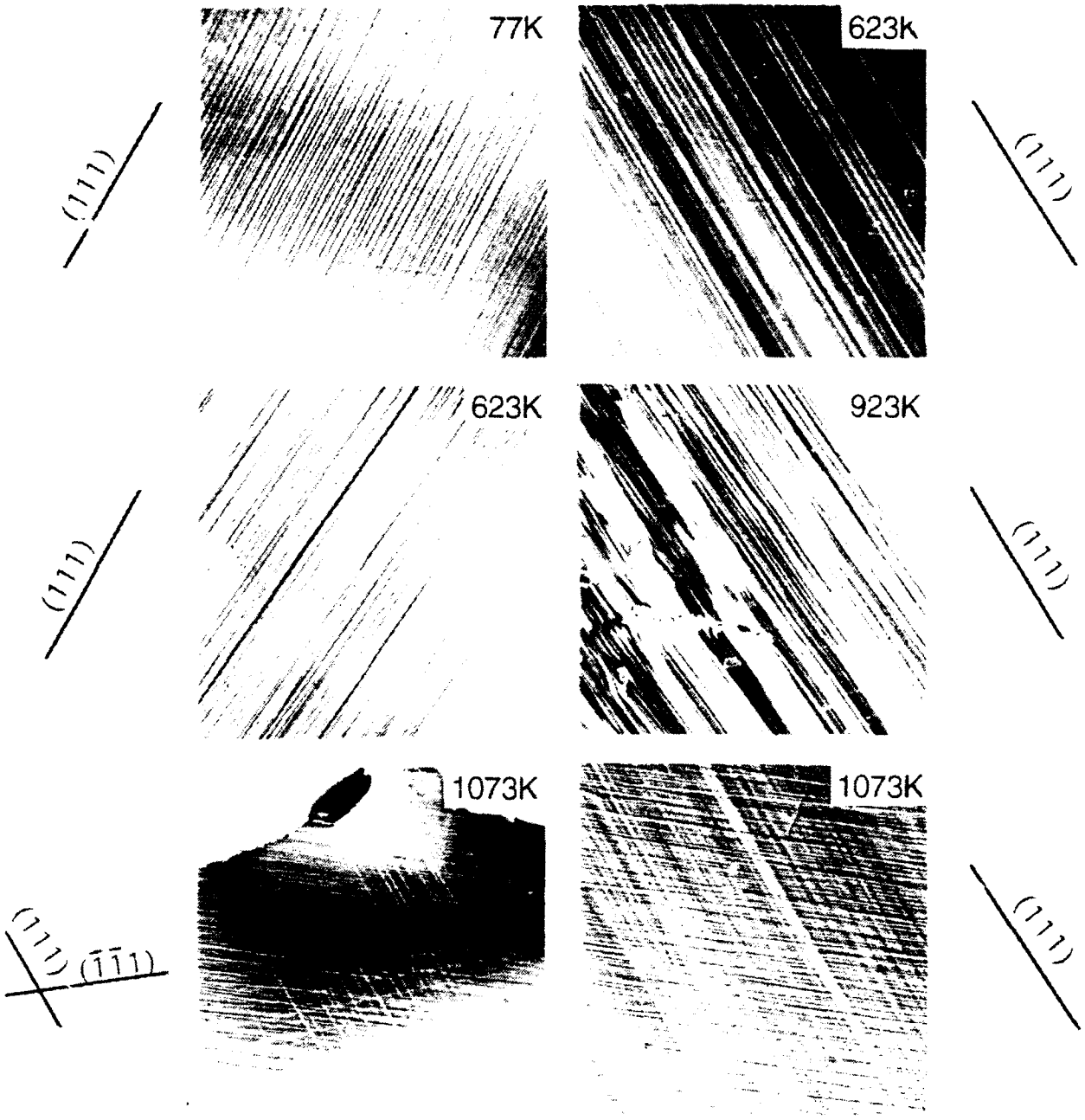

Fig. 10. Slip traces at various temperatures for **C1** test axis indicating octahedral slip.

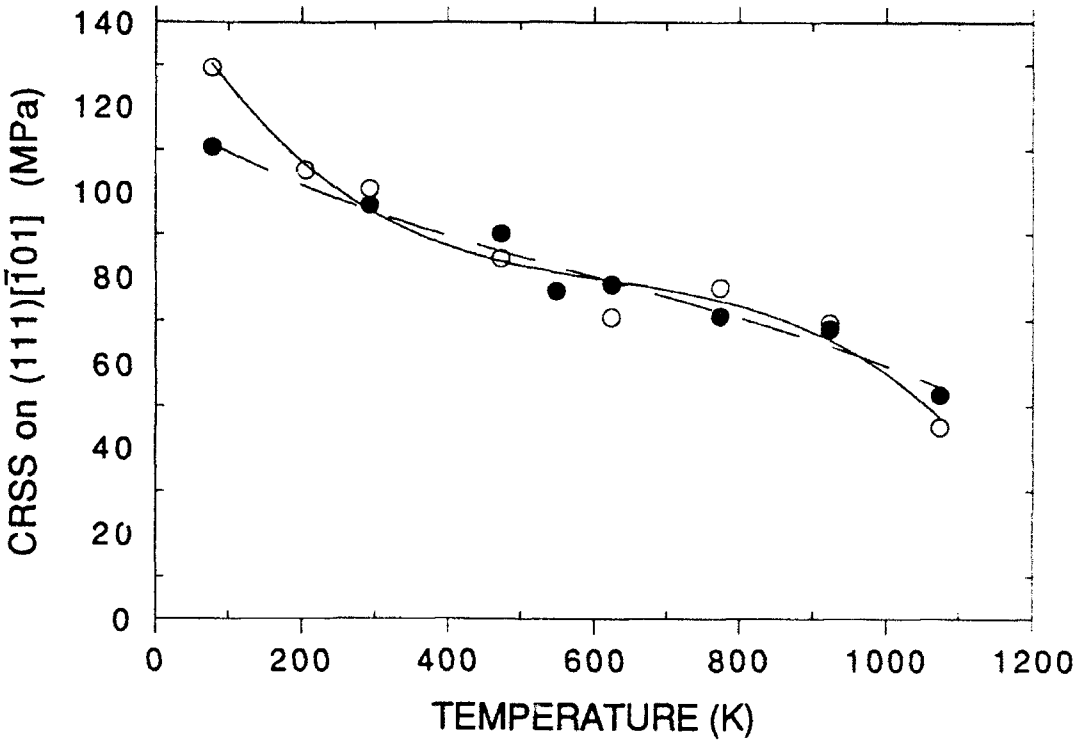

Fig. 11. CRSS versus temperature profiles for (111)[$\bar{1}$01] slip for both orientations (same symbols as Fig. 9).

g = [$\bar{1}1\bar{1}$], Z = [011]

g = [$0\bar{2}0$], Z = [001]

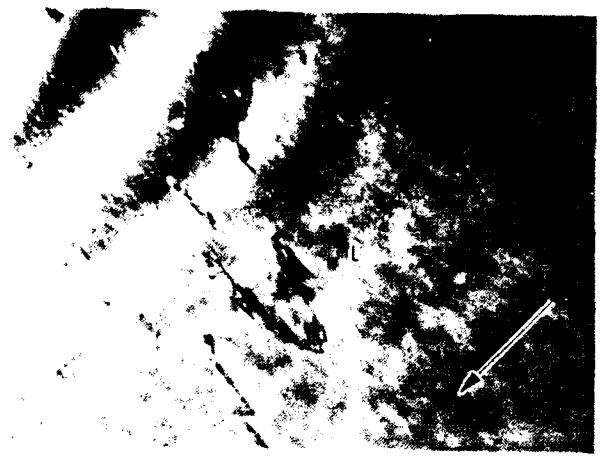

g = [$\bar{1}\bar{1}1$], Z = [011]

g = [$\bar{1}\bar{3}1$], Z = [$\bar{1}12$]

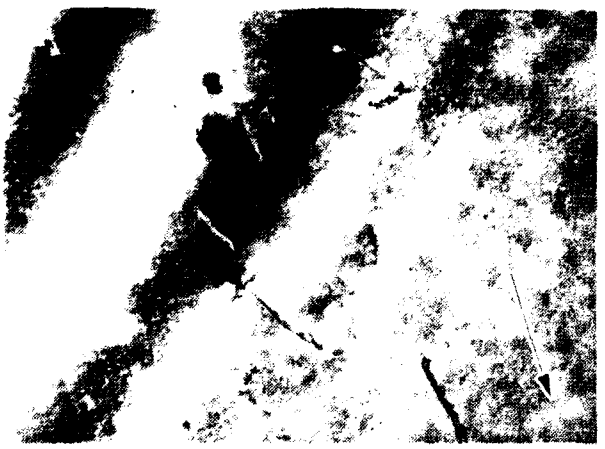

g = [$\bar{2}00$], Z = [011]

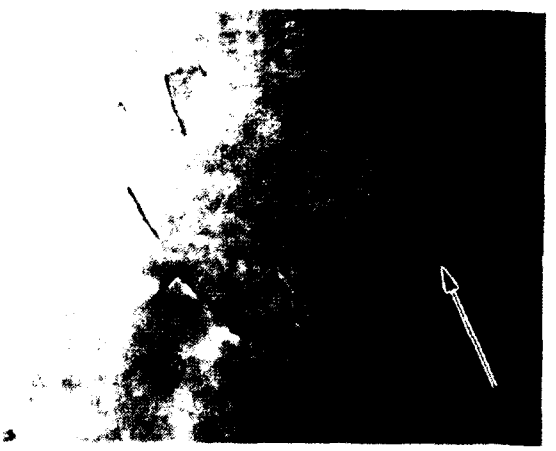

g = [200], Z = [001]

Fig. 12. Group of dislocations analyzed confirming a<110> type Burgers vectors at 298K for the **C1** compression axis, 1.0% strain.

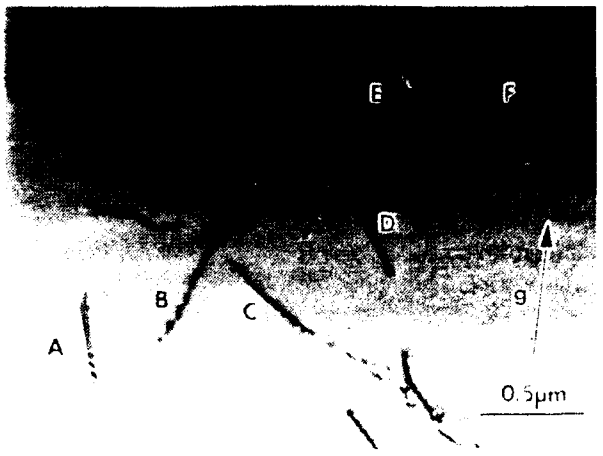

g = [1$\bar{1}$1], Z = [$\bar{1}$12]

g = [200], Z = [011]

g = [111], Z = [$\bar{1}$01]

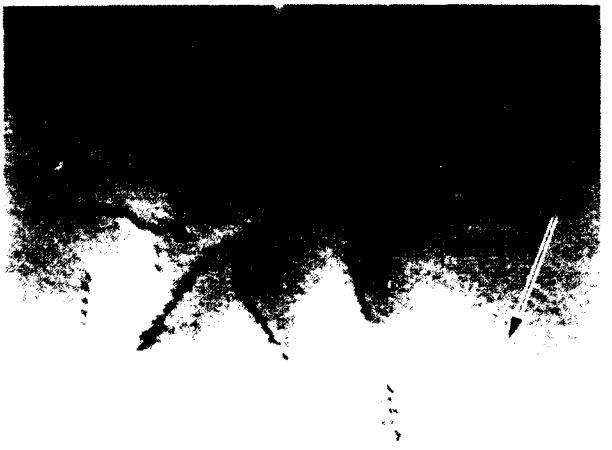

g = [$\bar{1}$1$\bar{1}$], Z = [$\bar{1}$01]

g = [020], Z = [001]

g = [11$\bar{1}$], Z = [011]

Fig. 13. Group of dislocations analyzed confirming a<110> type Burgers vectors at 1073K for the **C1** compression axis, 1.2% strain.

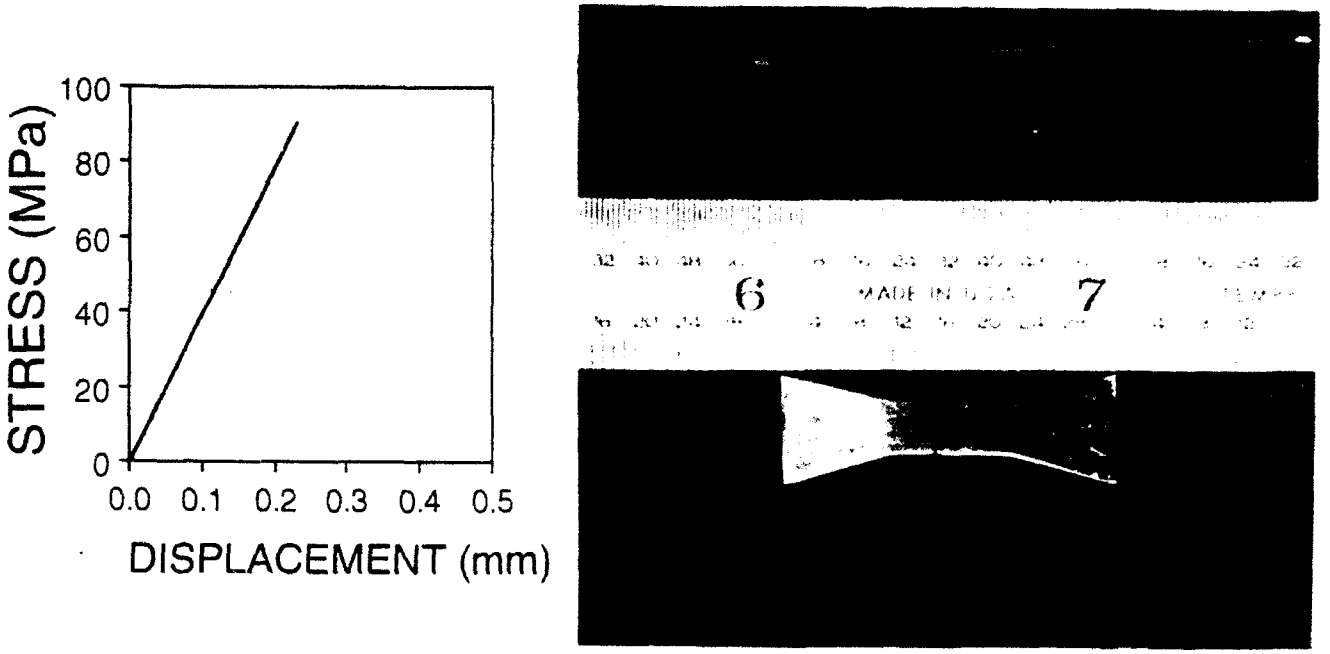

(a)

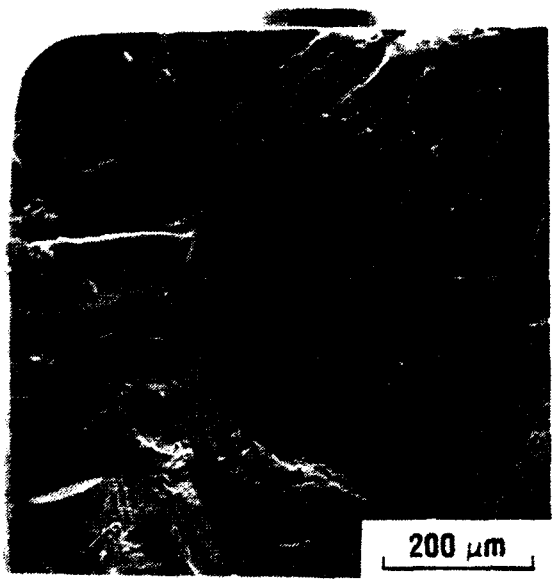

(b)

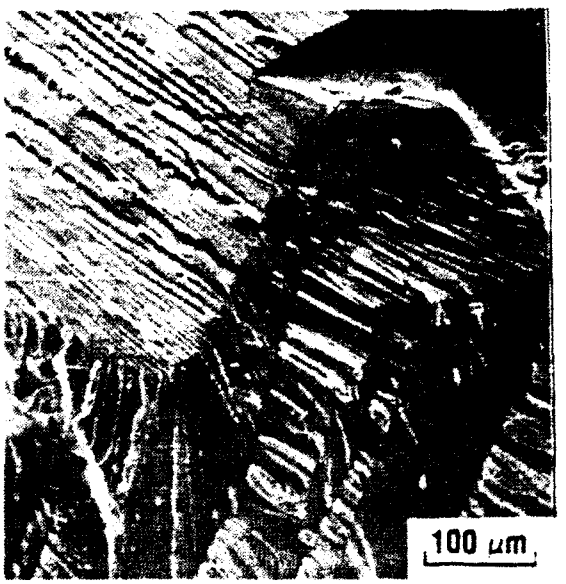

(c)

Fig. 14. Tensile testing results: (a) stress-displacement plot for 1073K tensile test and fractured specimen, (b) SEM micrograph of fracture surface at initiation corner, and (c) river patterns away from initiation site.